AMERICAN SOCIETY FOR MICROBIOLOGY | Antimicrobial Agents and Chemotherapy®

ANTIVIRAL AGENTS

Lancemaside A from *Codonopsis lanceolata*: Studies on Antiviral Activity and Mechanism of Action against SARS-CoV-2 and Its Variants of Concern

Tai Young Kim,[a] Sangeun Jeon,[b] Meehyun Ko,[b] Young Eun Du,[c] So-Ri Son,[d] Dae Sik Jang,[c,d] Seungtaek Kim,[b] C. Justin Lee[a]

[a]Center for Cognition and Sociality, Institute for Basic Science, Daejeon, South Korea
[b]Zoonotic Virus Laboratory, Institut Pasteur Korea, Seongnam, South Korea
[c]Department of Life and Nanopharmaceutical Sciences, Graduate School, Kyung Hee University, Seoul, South Korea
[d]Department of Biomedical and Pharmaceutical Sciences, Graduate School, Kyung Hee University, Seoul, South Korea

Tai Young Kim and Sangeun Jeon contributed equally to this work. Author order was determined in order of contribution.

ABSTRACT Several plant-derived natural products with anti-SARS-CoV-2 activity have been evaluated for the potential to serve as chemotherapeutic agents for the treatment of COVID-19. *Codonopsis lanceolata* (CL) has long been used as a medicinal herb in East Asian countries to treat inflammatory diseases of the respiratory system but its antiviral activity has not been investigated so far. Here, we showed that CL extract and its active compound lancemaside A (LA) displayed potent inhibitory activity against SARS-CoV-2 infection using a pseudotyped SARS-CoV-2 entry assay system. We demonstrated that this inhibitory effect of LA was due to the alteration of membrane cholesterol and blockade of the membrane fusion between SARS-CoV-2 and host cells by filipin staining and cell-based membrane fusion assays. Our findings also showed that LA, as a membrane fusion blocker, could impede the endosomal entry pathway of SARS-CoV-2 and its variants of concern (VOCs), including Alpha (B.1.1.7), Beta (B.1.351), Delta (B.1.617.2), and Omicron (B.1.1.529), in Vero cells with similar of IC_{50} values ranging from 2.23 to 3.37 μM as well as the TMPRSS2-mediated viral entry pathway in A549 cells overexpressing ACE2 and TMPRSS2 with IC_{50} value of 3.92 μM. We further demonstrated that LA could prevent the formation of multinucleated syncytia arising from SARS-CoV-2 spike protein-mediated membrane fusion. Altogether, the findings reported here suggested that LA could be a broad-spectrum anti-SARS-CoV-2 therapeutic agent by targeting the fusion of viral envelope with the host cell membrane.

KEYWORDS COVID-19, lancemaside A, Omicron, SARS-CoV-2, membrane fusion, triterpenoid saponin

During the ongoing coronavirus disease 2019 (COVID-19) pandemic, five variants of concern (VOCs) of the severe acute respiratory syndrome coronavirus 2 (SARS-CoV-2) were identified (1). The Alpha variant (lineage B.1.1.7) was first detected in the United Kingdom in early 2020 and then four additional variants, including Beta (B.1.351), Gamma (P.1), Delta (B.1.617.2), and Omicron (B.1.1.529), emerged and spread to many countries (2). Omicron, first reported to the World Health Organization (WHO) from South Africa on November 24, 2021, has now overtaken the previous variants and become the dominant variant around the world (3, 4). Changes in the dominant variant over time have been attributed to enhanced transmissibility of newly emerging variants over previous ones due to the additional mutation on spike (S) protein and its increased affinity to human receptor protein angiotensin-converting enzyme 2 (ACE2) (5, 6). These S mutations also confer resistance to antibody-based therapeutics and evasion from infection- and/or vaccine-induced humoral immunity (7–9). Thus, therapeutic strategies targeting common mechanisms that contribute to the infection of SARS-CoV-2 and their variants are imperative.

Address correspondence to Dae Sik Jang, dsjang@khu.ac.kr, Seungtaek Kim, seungtaek.kim@ip-korea.org, or C. Justin Lee, cjl@ibs.re.kr.

The authors declare no conflict of interest.

Received 3 September 2022
Returned for modification 28 September 2022
Accepted 18 October 2022
Published 14 November 2022

The entry of SARS-CoV-2 into human cells requires the binding of viral S protein to the ACE2 cellular receptor and subsequent fusion between the viral and cellular membranes, releasing the viral genome in the cytoplasm (10). The membrane fusion is mainly mediated by the S protein, which is comprised of two functional subunits termed S1 and S2, which are responsible for receptor binding and membrane fusion, respectively (11). Upon ACE2 binding, the S protein undergoes a conformational change from prefusion conformation to a postfusion structure via its proteolytic cleavage at S1/S2 sites by host cell proteases (10). The hydrophobic fusion peptide (FP) of the S2 subunit is exposed and inserted into host cell membranes, then the heptad repeat 1 (HR1) and 2 (HR2) domains in the S2 subunit are bound together to form a six-helix bundle (6-HB) fusion core, drawing the two membranes into proximity to facilitate virus-cell fusion (12). Because the S2 subunit is highly conserved across the coronavirus family, the FP and HR domains are considered key targets for the development of pan-coronavirus fusion inhibitors (12, 13). Previous studies have reported that HR2-derived peptides targeting the HR1 domain inhibit 6-HB formation, thereby blocking viral membrane fusion and cellular entry of human coronaviruses (14–16). It was also demonstrated that the conjugation of cholesterol to the peptide sequence leads to the anchoring of the peptide to the cell membrane where fusion occurs, strongly potentiating its action (12, 17).

Natural products have been an important source of recent drug development (18). Since the WHO declared COVID-19 as a pandemic, natural compounds have provided a wide array of potential anti-SARS-CoV-2 drug candidates with various cellular and viral targets. In line with this, we previously reported that platycodin D (PD), a natural component of *Platycodon grandiflorum* (PG), is capable of blocking SARS-CoV-2 infection (19). The roots of PG have been widely used to treat several respiratory diseases, such as asthma, airway inflammation, and sore throats (20, 21). Similarly, the roots of *Codonopsis lanceolata* (CL) have been widely used as a traditional medicinal herb in East Asian countries, such as Korea, China, and Japan, for the treatment of several disorders, including bronchitis, cough, and allergic lung inflammation (22, 23). It contains many biologically active compounds, including polyphenols, saponins, tannins, triterpene, alkaloids, and steroids (24). However, whether CL extracts or their active compounds may have inhibitory activity against viruses, including SARS-CoV-2 has not been investigated yet. In this study, we discovered that lancemaside A (LA), a triterpenoid saponin isolated from CL, effectively inhibited the infection of SARS-CoV-2 and its variants, including Alpha, Beta, Delta, and Omicron. We further found that LA affected the distribution of membrane cholesterol and blocked membrane fusion between SARS-CoV-2 and host cells to inhibit SARS-CoV-2 infection. These findings provide the first evidence that LA displays potent antiviral activity, particularly against SARS-CoV-2, and suggest the potential use of LA as a natural pan-coronavirus fusion inhibitor.

RESULTS

Triterpenoid saponins from *Codonopsis lanceolata* inhibits the infection of SARS-CoV-2. We first tested whether CL has an inhibitory activity against SARS-CoV-2 infection using a pseudovirus that expresses S protein on HIV-based lentiviral particles (pSARS-CoV-2), which has been used as a model system for analyzing SARS-CoV-2 infection (19, 25). pSARS-CoV-2 entry assay showed that the extracts of the roots and aerial parts of CL prevented pSARS-CoV-2 from entering the ACE2-overexpressing H1299 human lung carcinoma cells ($ACE2^+$ H1299) in a dose-dependent manner with half-maximal inhibitory concentrations (IC_{50}) of 251 μg/mL and 540 μg/mL, respectively, without obvious cell toxicity (Fig. 1A and B). These results indicated that CL extracts contained substances with inhibitory activity against SARS-CoV-2 infection, which was higher in the roots than in the aerial parts. To identify bioactive compounds in the CL, eight main compounds that we had previously isolated from the roots of CL (Fig. 1C) (24) were subjected to examinations for their inhibitory effects against two SARS-CoV-2 entry pathways, including endosomal pathway in $ACE2^+$ H1299 cells and TMPRSS2-mediated membrane fusion in ACE2 and TMPRSS2 double-positive cells

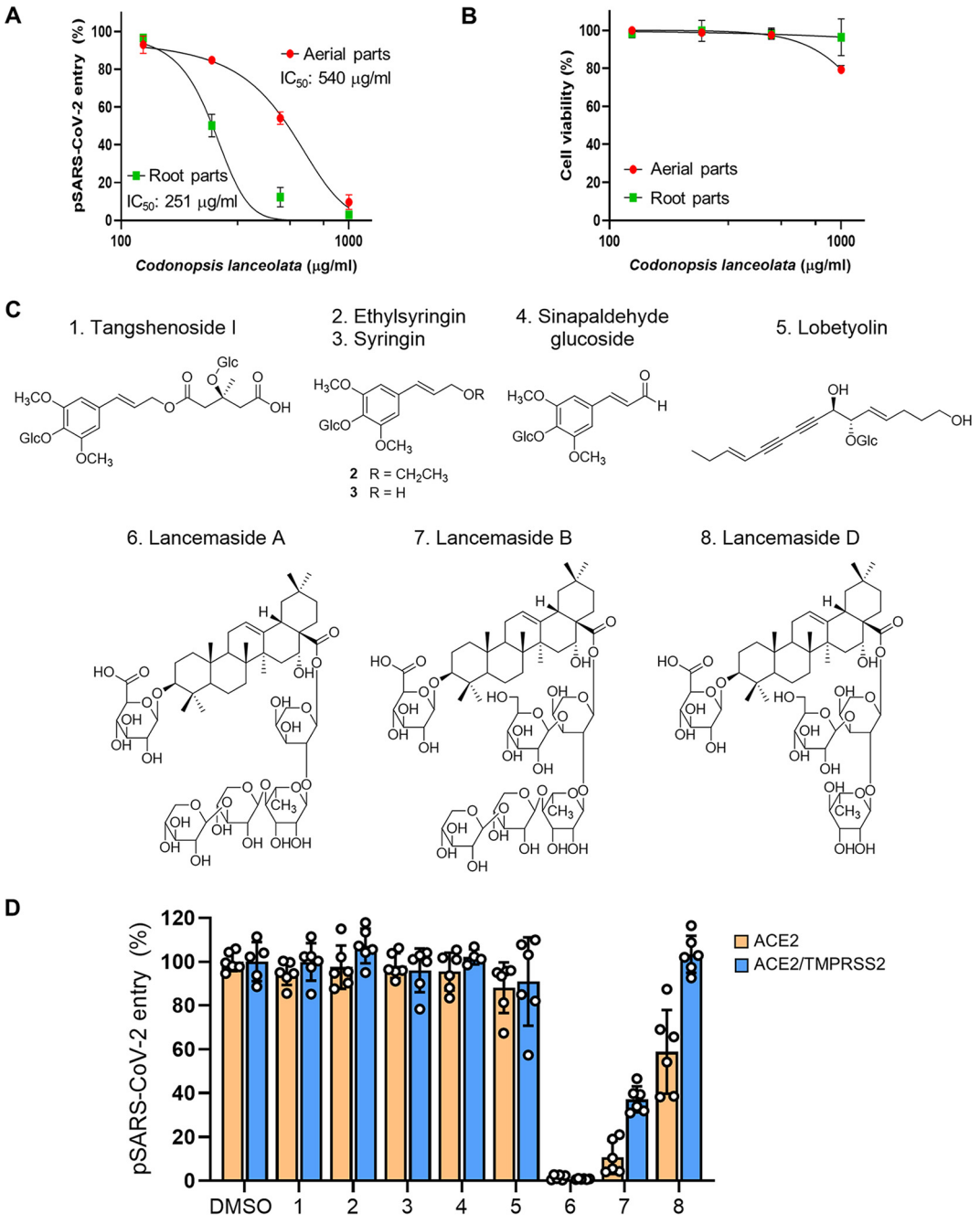

FIG 1 *Codonopsis lanceolata* extract and lancemaside A inhibit SARS-CoV-2 infection. (A) The effect of extracts from the aerial parts and roots of *Codonopsis lanceolata* (CL) on the entry of SARS-CoV-2 pseudovirus into ACE2$^+$ H1299 cells. The dried CL extracts were dissolved in DMSO at a concentration of 100 mg/mL as a stock solution. DMSO (1%) was used as solvent control. (B) The effect of the CL extracts on cell viability of H1299 cells. (C) The chemical structures of tangshenoside I (i), ethylsyringin (ii), syringin (iii), sinapaldehyde glucoside (iv), lobetyolin (v), lancemasides A (vi), B (vii), and D (viii) obtained from the roots of CL. (D) pSARS-CoV-2 entry assay with eight compounds described in (C) in ACE2$^+$ and ACE2/TMPRSS2$^+$ H1299 cells. DMSO (0.1%) was used as solvent control. All compounds were used at the concentration of 10 μM.

(ACE2/TMPRSS2$^+$ H1299). Our results revealed that pentacyclic triterpenoid saponins, such as lancemaside A (LA) and lancemaside B (LB) but not lacemaside D (LD), effectively blocked both SARS-CoV-2 entry pathways (Fig. 1D), indicating that LA and LB are biologically active compounds responsible for the anti-SARS-CoV2 activity of CL extracts.

Lancemaside A is a potent antiviral agent that inhibits two main SARS-CoV-2 entry pathways. Next, we further evaluated the inhibitory activity of three triterpenoid saponins against pSARS-CoV-2 entry at various concentrations and obtained the IC_{50} values of 1.77, 4.97, and 39.76 μM for LA, LB, and LD in ACE2$^+$ H1299 cells (Fig. 2A). Based on these findings, LA was chosen for further experiments. We extended our analysis to examine the effect of LA against the infection of authentic SARS-CoV-2 into Vero cells that express high levels of ACE2 but no detectable TMPRSS2 (19). Assessment of SARS-CoV-2 infection based on immunostaining of SARS-CoV-2 nucleocapsid (N) protein in Vero cells showed that LA exhibited antiviral activity against ancestral SARS-CoV-2 with IC_{50} of 2.62 μM (Fig. 2B). Importantly, LA was found to be more effective than remdesivir, an FDA-approved anti-SARS-CoV-2 drug (IC_{50}, 7.24 μM) (Fig. 2C). However, the potency of remdesivir is highly cell line-dependent and varies depending on the assessment method (26), thus it cannot be concluded that LA is more potent than remdesivir. Moreover, we verified the inhibitory activity of LA against the TMPRSS2-dependent cell surface entry pathway of SARS-CoV-2 by measuring the entry of pSARS-CoV-2 into ACE2/TMPRSS2$^+$ H1299 cells (Fig. 2D) and the infection of a recombinant SARS-CoV-2 reporter virus expressing the nanoluciferase (Nluc) (SARS-CoV-2-Nluc) into A549 cells that overexpress both ACE2 and TMPRSS2 (ACE2/TMPRSS2$^+$A549). (Fig. 2E). The results showed that LA effectively blocked SARS-CoV-2 entry in these cells with an IC_{50} of 2.85 and 3.92 μM, respectively (Fig. 2D and E). Overall, these results confirm that LA is the most potent antiviral agent among the triterpenoid saponins from CL extracts and restricts SARS-CoV-2 entry both at the endosomal compartments and at the cell surface.

Protein interaction between S protein and ACE2 is not the main target for lancemaside A to inhibit SARS-CoV-2 infection. Having observed that LA inhibited two main SARS-CoV-2 entry routes to a similar extent, we reasoned that a possible target for LA could be a common step of both viral entry pathways. Therefore, we first examined the effect of LA on the interaction between SARS-CoV-2 S protein and ACE2. To do so, a recombinant protein containing receptor-binding domain (RBD) of the SARS-CoV-2 S protein fused with a green fluorescent protein (GFP) (S-RBD-GFP) was produced and added into ACE2$^+$ H1299 cells (Fig. 3A). Flow cytometry showed that more than 97% of the cells were bound with S-RBD-GFP (Fig. 3B), reflecting SARS-CoV-2 S attachment to a cellular receptor for viral cell entry. Importantly, pretreatment of ACE2$^+$ H1299 cells with CL root extracts or LA did not affect the binding of S-RBD-GFP to ACE2 on the cells within the effective concentration range we obtained in the pSARS-CoV-2 entry assays (Fig. 1A and 2A), despite somewhat inhibitory effects were seen at higher concentrations (Fig. 3B). Moreover, LB, LD, and triterpenoid aglycone such as echinocystic acid (EA) did not display any inhibitory effects until their concentration reached 20 μM (Fig. 3C). Overall, these results suggest that S-ACE2 protein-protein interaction is not the main target for LA to inhibit SARS-CoV-2 infection.

Lancemaside A inhibits SARS-CoV-2 entry by blocking S protein-mediated viral membrane fusion. As a next step, we tested the possibility that LA may prevent fusion between the viral and host membranes, a process that commonly occurs in both entry pathways. For the assay, we established two stable cell lines: one that overexpresses S protein with EGFP from a single bicistronic mRNA in HEK293T cells (Spike-HEK293T) and the other overexpressing mRuby in ACE2/TMPRSS2$^+$ H1299 cells. Then, dual imaging time-lapse microscopy was performed to monitor cell fusion between these two cells as indicative of the S-mediated membrane fusion during viral entry (Fig. S1 in Supplemental File 1). The addition of Spike-HEK293T cells to a monolayer of ACE2/TMPRSS2$^+$ H1299 rapidly induced the cell-to-cell fusion, which allows them to fuse continuously with neighboring ACE2/TMPRSS2$^+$ H1299 due to the S protein displayed on the surface of fused hybrid cells, eventually giving rise to enlarged multinucleated cells (Fig. 4A). The heterologous cell fusion was mediated by the interaction between S protein and ACE2 because this process was not observed in coculture of HEK293T expressing GFP only with ACE2/TMPRSS2$^+$ H1299 cells (Fig. 4A). We next examined the effects of LA on the cell-to-cell fusion event. Strikingly, pretreatment with 10 μM LA almost completely blocked the fusion of Spike-HEK293T cells with ACE2/TMPRSS2$^+$

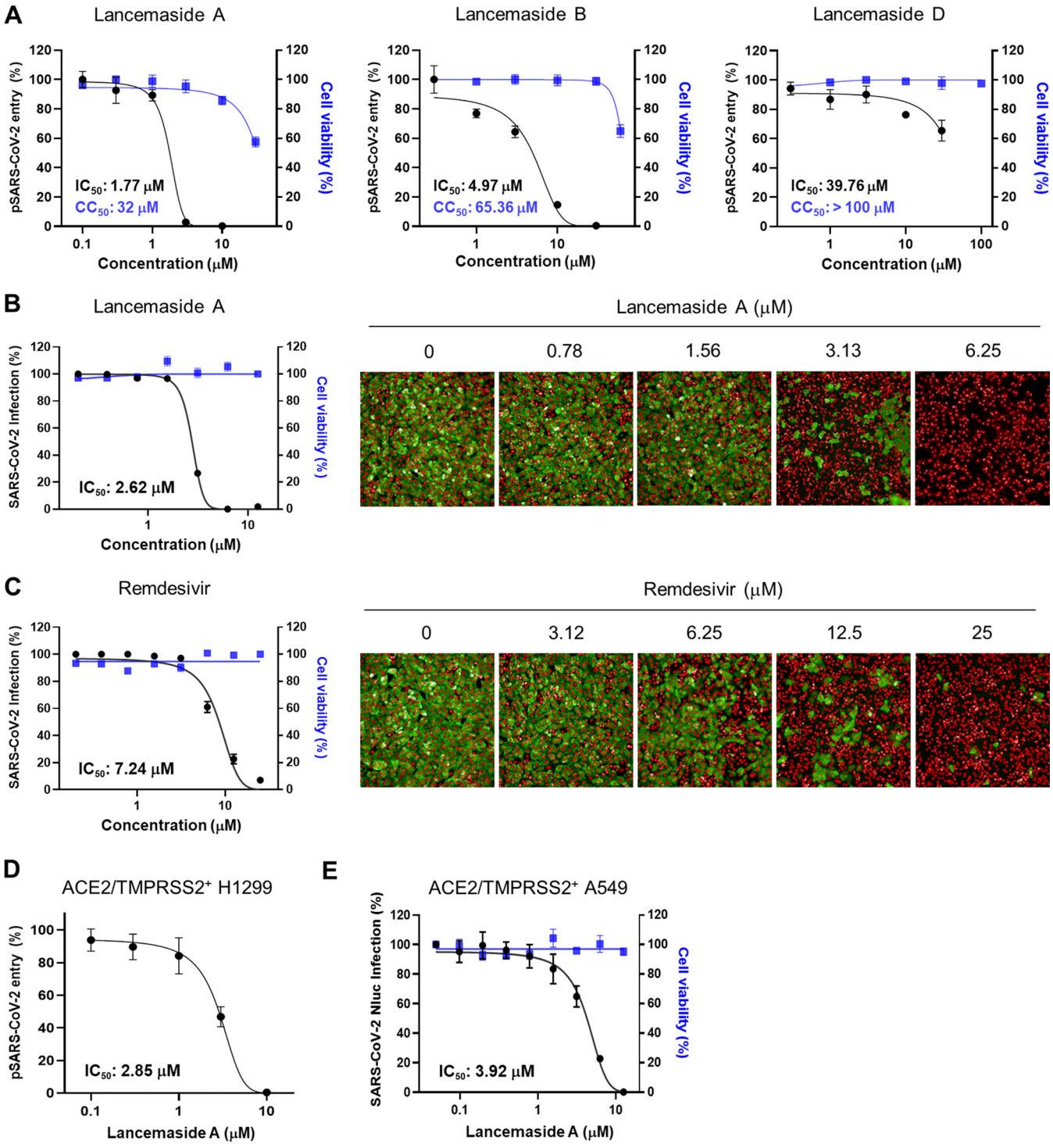

FIG 2 Lancemaside A inhibits both endocytic and TMPRSS2-mediated SARS-CoV-2 entry pathways. (A) The effects of LA, LB, and LD on the entry of pSARS-CoV-2 into ACE2$^+$ H1299 cells (black circle) and cell viability (blue square). The 50% inhibitory concentration (IC_{50}) and 50% cytotoxic concentration (CC_{50}) for each compound are indicated in the graphs. The data were representative of three independent experiments with triplicate samples. The error bars indicate the SEM. (B and C) Dose-response curves and confocal images of SARS-CoV-2 N protein (green) and cell nuclei for LA (B) and remdesivir (C) on the infection of ancestral SARS-CoV-2 (black circle) in Vero cells. The blue squares represent Vero cell viability. (D) The effects of LA on the entry of pSARS-CoV-2 into ACE2/TMPRSS2$^+$ H1299 cells. (E) Dose-response curve for LA against SARS-CoV-2 recombinant viruses expressing nanoluciferase (Nluc) into A549 cells overexpressing both ACE2 and TMPRSS2. The blue squares represent A549 cell viability. DMSO (0.1%) was used as solvent control. The mean ± SEM was calculated from duplicate experiments. The error bars are not visible when they are within the symbols.

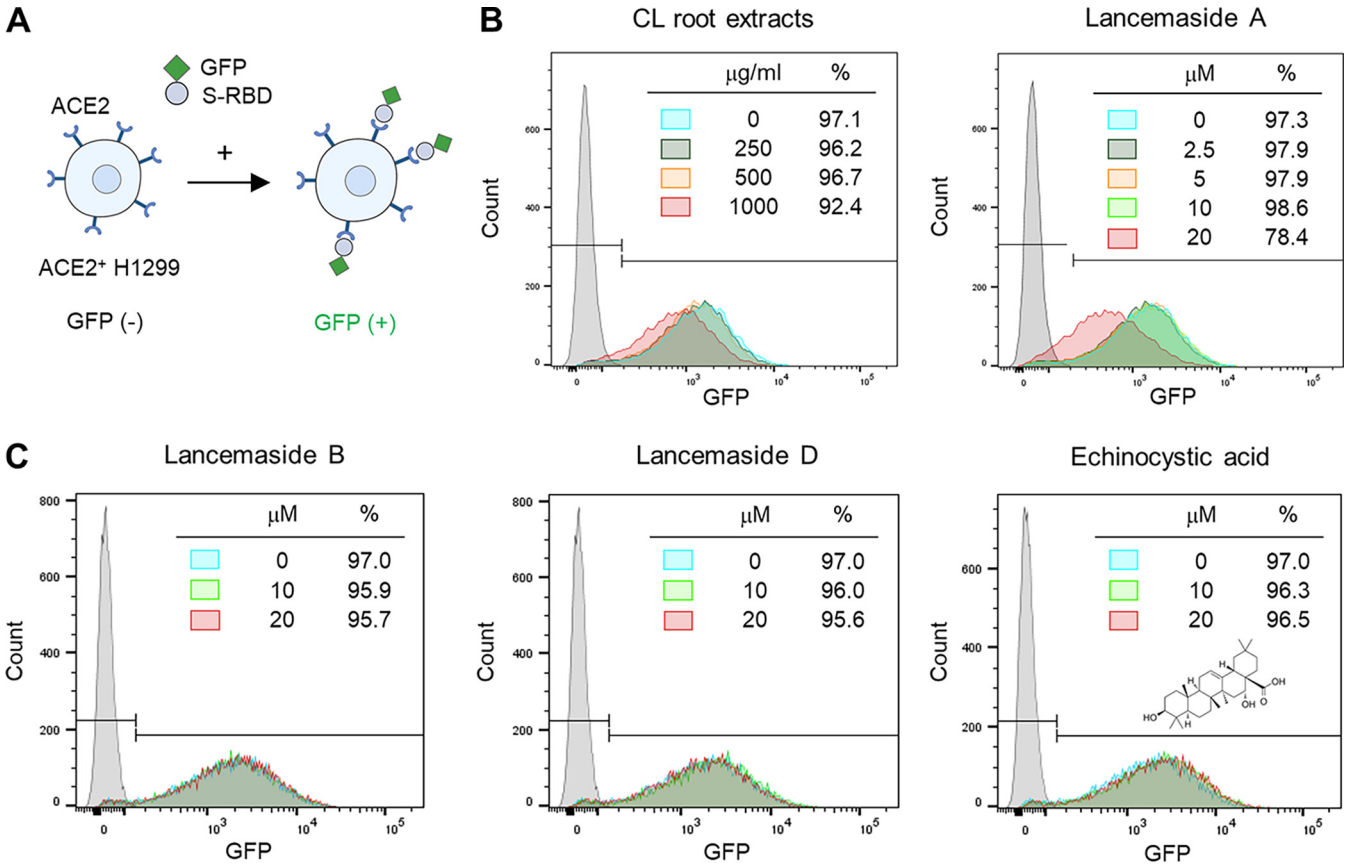

FIG 3 The effects of natural compounds isolated from CL on the binding of SARS-CoV-2 S protein to ACE2. (A) Schematics for SARS-CoV-2 Spike-ACE2 binding assay using S-RBD-GFP, a recombinant protein comprised of receptor binding domain (RBD) of S protein fused to GFP and ACE2$^+$H1299 cells. (B and C) The binding of S-RBD-GFP to ACE2 overexpressed on the surface of H1299 cells was determined by flow cytometry after pretreatment with the indicated concentration of CL root extracts, lancemaside A (B), lancemaside B, lancemaside D, and echinocystic acid (C). DMSO (0.1%) was used as solvent control. The gray peaks indicate the control experiments without S-RBD-GFP addition. The same control data were used for each flow cytometry plot.

H1299 cells (Fig. 4A), implicating impairment of SARS-CoV-2 entry by LA at the membrane fusion step. Furthermore, we quantified the cell-to-cell fusion by flow cytometry analysis after coculturing the two cell types in a ratio of 1 to 3. The results showed that approximately 30% of total cells were double-positive for mRuby and GFP, indicating that most of Spike-HEK293T cells participated in the fusion event (Fig. 4B). Meanwhile, the double-positive cells were barely detected when control GFP-HEK293T cells (no S protein) were cocultured with ACE2/TMPRSS2$^+$ cells, again demonstrating the requirement of S protein during the cell-to-cell fusion (Fig. 4B). Notably, pretreatment with 10 μM LA strongly blocked the fusion event, with less than 4% of cells generating cell fusion hybrids (Fig. 4B). On the other hand, LB and LD showed less or no anti-fusion activity (Fig. 4B), further supporting our results obtained in pSARS-CoV-2 entry assay (Fig. 2A). Next, we investigated how LA may affect membrane fusion. We previously reported that PD, a triterpenoid saponin derived from PG, redistributes membrane cholesterol and inhibits SARS-CoV-2 infection (19). Membrane cholesterol is an essential component for SARS-CoV-2 to enter the host cells through membrane fusion (27). Because LA has a similar chemical structure to PD, we reasoned that LA might also alter membrane cholesterol content and undertook confocal microscopy analysis of filipin staining to investigate membrane cholesterol distribution after LA treatment. We found that 1 h treatment of ACE2$^+$ H1299 cells with 10 μM LA significantly led to an increase in cholesterol content at the plasma membrane (Fig. 4C and D). Importantly, these redistributions of cholesterol were also observed upon treatment of parental H1299 cells with LA (Fig. 4C and D), indicating that LA affected cell membranes directly and not by affecting ACE2. Moreover, we treated ACE2$^+$ H1299 cells with LB, LD, and

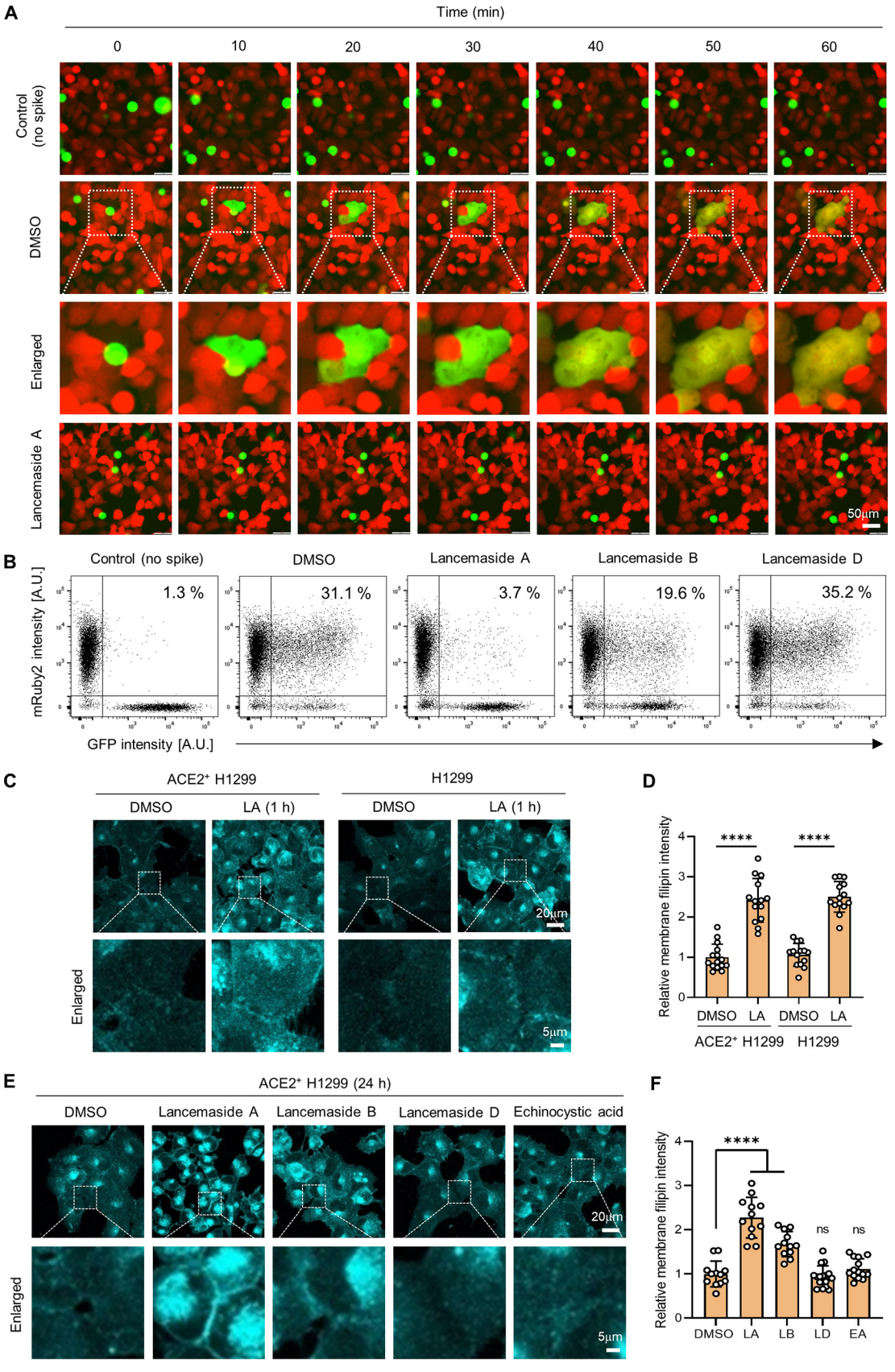

FIG 4 Lancemaside A blocks SARS-CoV-2 S-mediated membrane fusion. (A and B) The effect of natural compounds on membrane fusion between Spike-HEK293T (EGFP$^+$) and ACE2/TMPRSS2$^+$ H1299 (mRuby2$^+$) cells was monitored by time-lapse

(Continued on next page)

EA for 24 h, and compared their effects on membrane cholesterol with that of LA. The cells showed that LB also increased the amount of cholesterol in the plasma membrane by about 1.7-fold above DMSO-treated control, as revealed by filipin staining, but it was lower than that of LA (2.3-fold increase) (Fig. 4E and F). But, LD and EA did not show any effects on membrane cholesterol content (Fig. 4E and F). Intriguingly, the altered levels of membrane cholesterol caused by these triterpenoid saponins were well correlated with their inhibitory ability against S-mediated membrane fusion and viral entry (Fig. 3B and Fig. 2A), supporting the idea that membrane cholesterol might be a direct target for LA to exert its anti-SARS-CoV-2 activity. Moreover, cholesterol in intracellular vesicles was also greatly increased by LA and LB treatment (Fig. 4E) and colocalized with endosomal and lysosomal markers (Fig. S2 in Supplemental File 1), indicating that the endosomal entry pathway of SARS-CoV-2 was also impeded due to high cholesterol levels in the endosomal and lysosomal membranes. Taken together, our data suggest that LA interferes with the S-mediated membrane fusion, possibly by altering the distribution of cholesterol on the host cell membrane, leading to the inhibition of main SARS-CoV-2 infection routes.

Lancemaside A blocks syncytium formation. Given that LA has an inhibitory activity for membrane fusion, we next sought to investigate the effects of LA on the formation of multinucleated giant cells called syncytia, which was a result of the continuous fusion of SARS-CoV-2-infected cells with neighboring cells and often detected in lung tissue from COVID-19 patients (28, 29). For the assay, we employed a split-GFP complementation technology, in which half of GFP was expressed separately in different cells and a functional GFP protein can be reconstituted upon cell-to-cell fusion. ACE2/TMPRSS2$^+$ H1299 cells stably expressing each of the two fragments of the reporter protein were generated and plated in equal numbers, and then S protein was ectopically expressed in these cell mixtures to induce syncytium formation, which can be detected by GFP fluorescence (Fig. 5A and B). In DMSO-treated control cells, multiple enlarged GFP$^+$ cells with clustered nuclei were detected, indicating syncytia were formed (Fig. 5C, upper). Using automated image analysis, we quantified the efficiency of syncytium formation by dividing the number of nuclei into GFP$^+$ multinucleated cells by the total number of nuclei in the field of view (Fig. 5C, lower) and found that approximately 30% of the total number of cells plated formed GFP$^+$ syncytia (Fig. 5D). Importantly, the number of GFP$^+$ cell clusters was dose-dependently reduced by LA treatment with IC_{50} values of 3.94 μM, indicating that LA effectively inhibited the S-mediated syncytium formation (Fig. 5C and D). Note that LA did not exhibit a significant inhibitory activity at a concentration close to its IC_{50} value obtained from the pSARS-CoV-2 entry assay (Fig. 2D), indicating that cell-to-cell fusion might occur with higher probability compared to virus-to-cell fusion and, thus, higher concentrations of LA were needed to block the S-mediated syncytium formation. Because virus-induced syncytium formation generally promotes programmed cell death (30, 31), we next asked if LA could prevent the viral activation of apoptotic pathways. Consistent with previous studies, the S-mediated syncytia promoted apoptosis as evidenced by Western blotting of the proteolytic cleavage of caspase 3 and 9 (Fig. 5E). Notably, these apoptotic markers were not detected under no S expression and LA pretreatment conditions (Fig. 5E). Overall, these results indicate that LA blocks the S-induced syncytium formation and consequent apoptotic cell death.

FIG 4 Legend (Continued)
microscopy (A) and determined by counting the number of EGFP/mRuby2 double positive cells by flow cytometry (B). EGFP-HEK293T cells (no spike) were used for the control experiment. All compounds were used at the concentration of 10 μM. The data were representative of three independent experiments. (C and D) Filipin staining of intracellular cholesterol in ACE2$^+$ H1299 and parental H1299 cells after treatment with DMSO or 10 μM LA for 1 h (C) and quantification of the membrane cholesterol levels using Image J (n = 14 for each group) (D). (E and F) Filipin staining of intracellular cholesterol in ACE2$^+$ H1299 cells after treatment with DMSO, 10 μM lancemaside A (LA), lancemaside B (LB), lancemaside D (LD), and echinocystic acid (EA) for 24 h (E). Quantification of the membrane cholesterol levels using Image J (n = 12 -15 for each group) (F). DMSO (0.1%) was used as solvent control. Error bars in the graphs indicate the SEM. P values were determined by the unpaired, two-tailed Student's t test. ****, $P < 0.0001$.

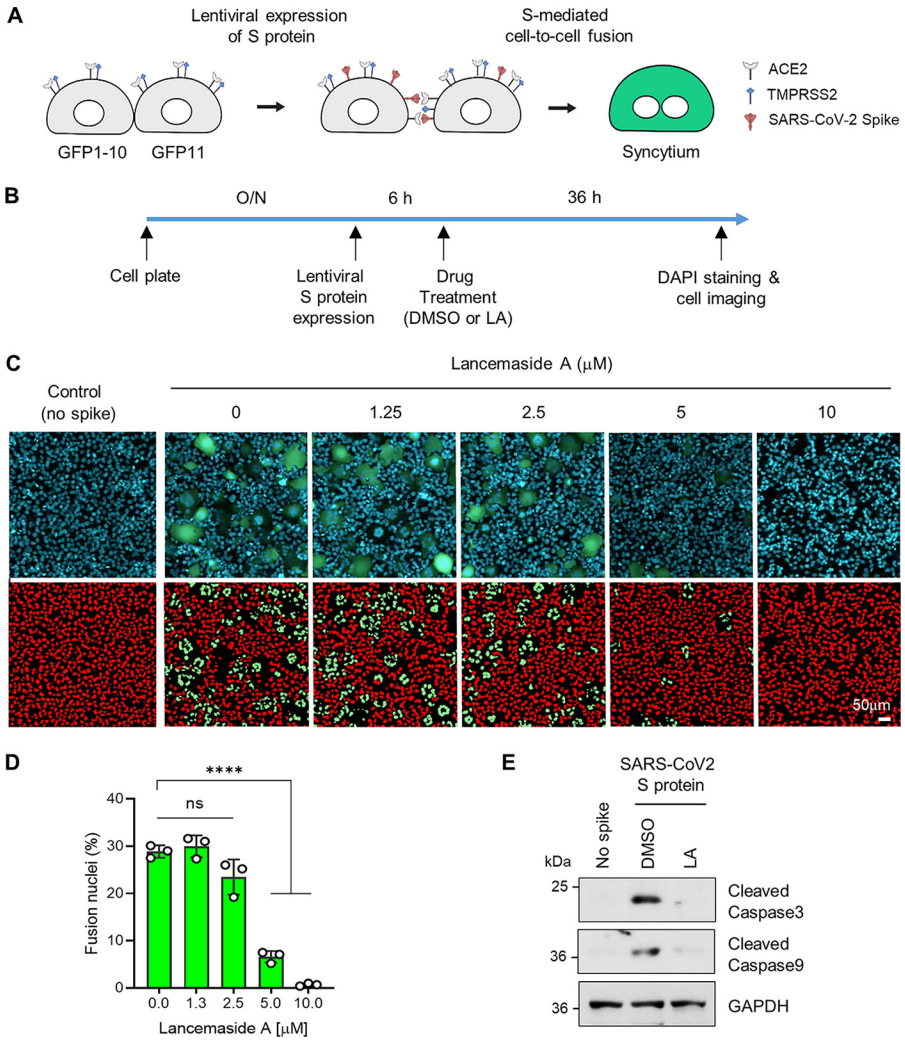

FIG 5 Lancemaside A inhibits S-mediated syncytium formation. (A) Schematic diagram of the Split-GFP assay to monitor syncytium formation. (B) Experimental timeline for the split-GFP fusion assay. (C) GFP and DAPI (blue) fluorescent images indicate syncytia formed by cell-to-cell fusion and cell nuclei, respectively (upper). DAPI nuclear staining overlapped and nonoverlapped with GFP fluorescence are pseudocolored in green and red, respectively (lower). (D) Quantitative assessment of syncytium formation. GFP and DAPI images were obtained in three random fields per well and the percentage of syncytium formation was calculated by dividing the number of nuclei into GFP-positive cells by the total number of nuclei. DMSO (0.1%) was used as solvent control. The data were representative of three independent experiments. The error bars indicate the SEM. *P* values were determined by ANOVA followed by Tukey's *post hoc* test. ****, $P < 0.0001$; NS not significant. (E) Western blot analysis using protein lysates from split-GFP experiments (incubation time was 72 h) with anti-cleaved caspase-3 and -9 antibodies. GAPDH was used as a loading control.

Lancemaside A effectively inhibits SARS-CoV-2 infection regardless of S mutation. Mutations in gene encoding S protein, which were found in most SARS-CoV-2 variants, have been reported to cause an increase in SARS-CoV-2 infectivity by enhancing attachment to ACE2 on the host cell surface (32–34). Among novel S mutations, D614G was the most common one found in lineage B.1 of SARS-CoV-2 including Alpha, Beta, Delta, and Omicron variants (35). To test whether LA can equally inhibit the enhanced SARS-CoV-2 infectivity mediated by S mutations, the D614G mutation was introduced into the S gene by site-directed mutagenesis. Consistent with previous studies, pSARS-CoV-2 carrying the D614G mutation showed significantly higher infectivity compared to the wild-type (WT) (36) in both ACE^+ and $ACE2/TMPRSS2^+$ H1299 cells (Fig. 6A). Importantly, LA treatment blocked the entry of the D614G mutant virus with IC_{50} of 2.02 and 2.99 μM in $ACE2^+$ and $ACE2/TMPRSS2^+$ H1299 cells, respectively

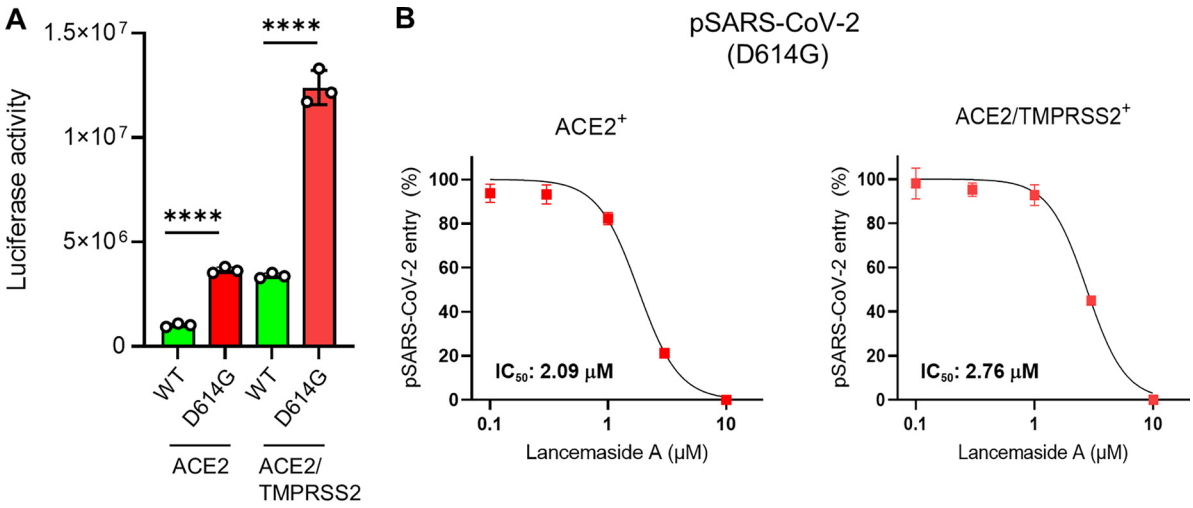

FIG 6 Lancemaside A inhibits the infection of SARS-CoV-2 WT and D614G mutant. (A) The entry levels of WT and D614G mutant of pSARS-CoV-2 into ACE2$^+$ and ACE2/TMPRSS2$^+$ H1299 cells. *P* values were determined by the unpaired, two-tailed Student's *t* test (****, $P < 0.0001$). (B) The effects of LA on the infection of WT and D614G mutant of pSARS-CoV-2 in ACE2$^+$ and ACE2/TMPRSS2$^+$ H1299 cells. DMSO (0.1%) was used as solvent control. The data from the pSARS-CoV-2 entry assay were representative of three independent experiments with triplicate samples. The error bars indicate the SEM. The error bars are not visible when they are within the symbols.

(Fig. 6B), which were comparable to those of the WT virus (Fig. 2A and D), indicating that LA effectively inhibits SARS-CoV-2 infection regardless of S mutation.

Lancemaside A displays inhibitory activity against SARS-CoV-2 variants. We next sought to investigate whether LA could inhibit SARS-CoV-2 variants by imaging SARS-CoV-2 N protein in Vero cells 24 h after the inoculation of the authentic virus. The results showed that LA treatment impeded the infection of SARS-CoV-2 variants, including Alpha, Beta, Delta, and Omicron with similar IC_{50} values of 3.37, 3.12, 2.23, and 2.45 μM, respectively (Fig. 7A). Importantly, these values were comparable to that of ancestral virus (IC_{50}, 2.62 μM) (Fig. 2B), providing further corroborating evidence that LA could effectively hinder the infection of SARS-CoV-2 regardless of the types of S-mutation. Of note, remdesivir exhibited less effective and variable inhibitory activity toward SARS-CoV-2 variants (IC_{50}, 4.06 to 7.40 μM) compared to LA (Fig. 7B). Again, the activity of remdesivir was reported to be highly cell line-dependent due to its identity as a prodrug, and to retain its antiviral activity against SARS-CoV-2 variants of concern (37, 38). Together, these results demonstrate that LA blocks the infection of SARS-CoV-2 variants, as well as their ancestral virus, with similar efficiency and, thus, implicate that LA could be a broad-spectrum antiviral agent, providing additional protection strategy against infection by SARS-CoV-2 variants.

DISCUSSION

Since the outbreak of the COVID-19 pandemic, numerous single herbs and herbal formulations as well as single compounds isolated from the herbal extracts have been reported to exhibit significant anti-SARS-CoV-2 effects through the inhibition of SARS-CoV-2 life cycle by targeting viral proteins, such as 3CLpro, PLpro, RNA-dependent RNA polymerase (RdRp), and S protein, and cellular proteins such as ACE2, cathepsin L, and TMPRSS2 (39–41). Saponins, including triterpenoid saponins derived from various medicinal plants, have also been investigated for their therapeutic potential against SARS-CoV-2 (42). However, most are based on *in silico* studies (43–46), and it was only recently that their inhibitory activities have been demonstrated using pseudotyped or authentic SARS-CoV-2. Licorice-saponin A3, a triterpenoid saponin isolated from licorice, was reported to inhibit SARS-CoV-2 by targeting the NSP7, a core component of RdRp (47). Hui et al. (48) recently showed that the 3-O-β-chacotriosyl ursolic acid saponins they synthesized displayed anti-SARS-CoV-2 activity by binding to S protein. However, to our knowledge, there have been few studies verifying the role of natural

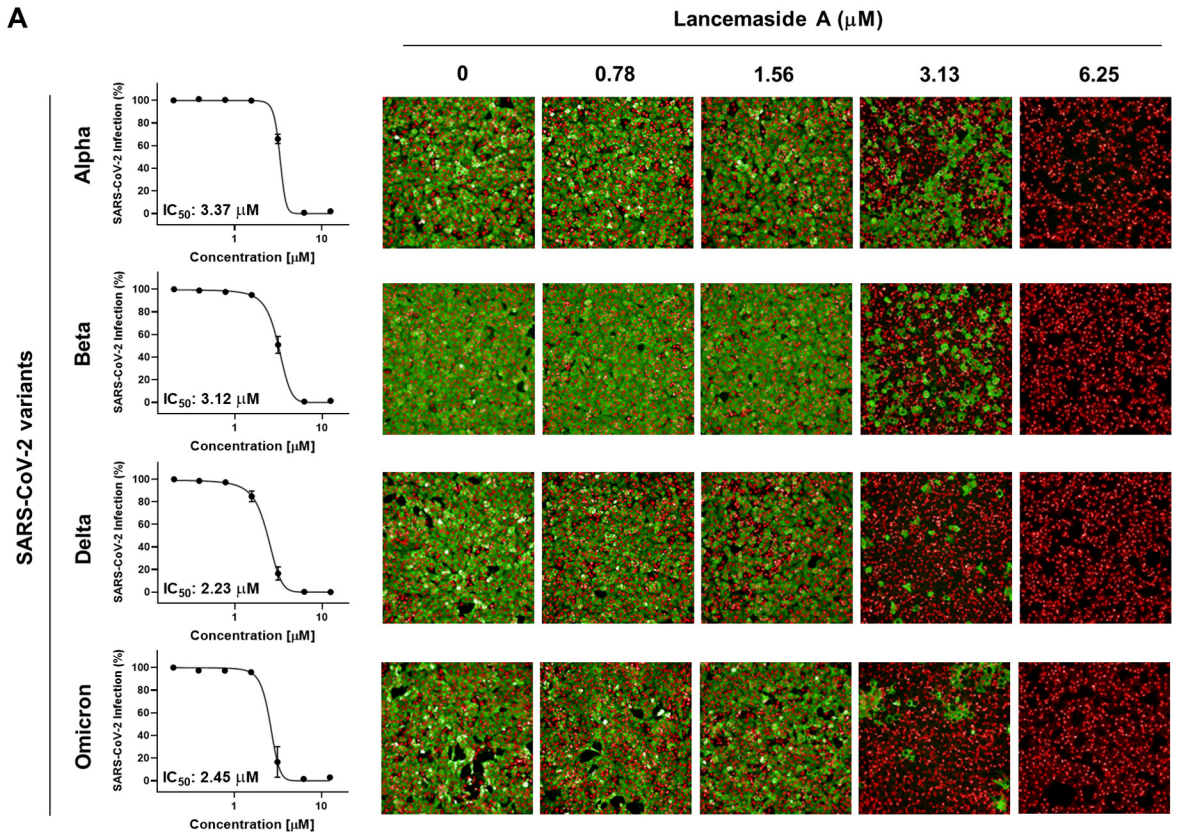

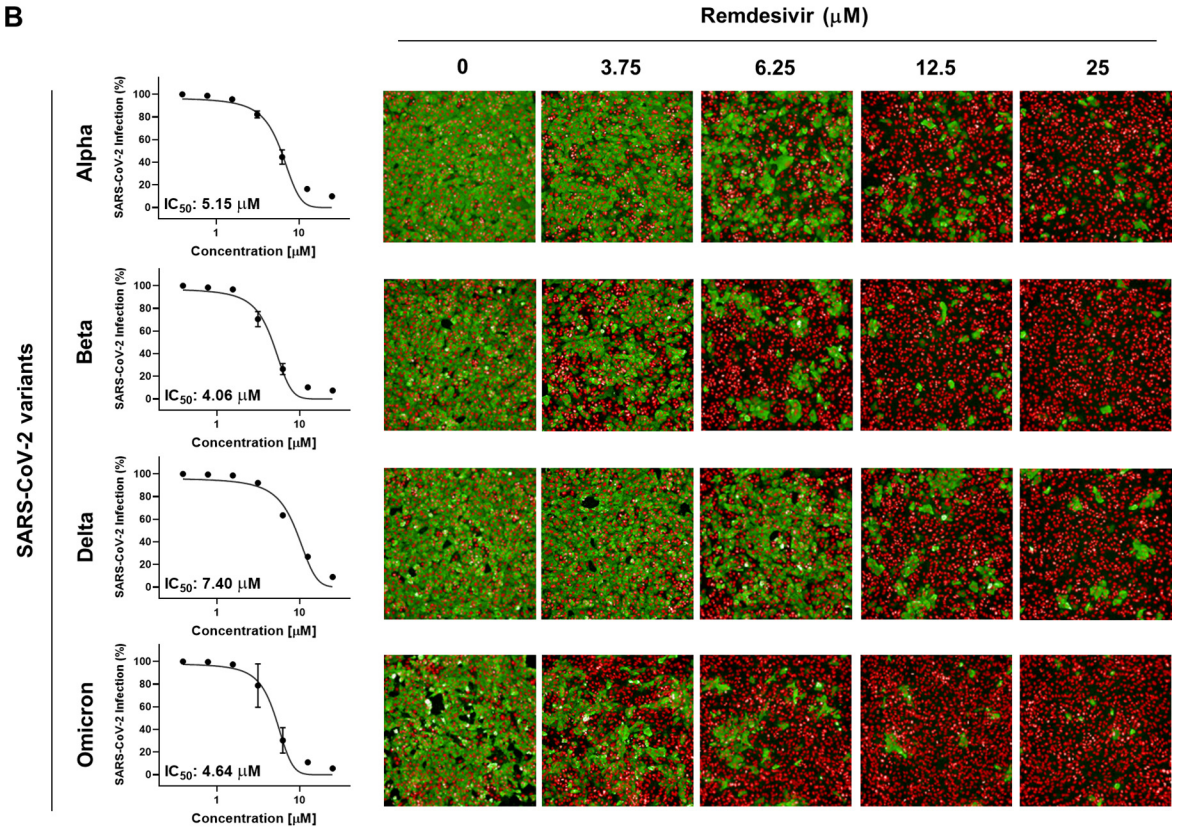

FIG 7 Lancemaside A effectively inhibits the infection of SARS-CoV-2 variants (A and B) Dose-response curves for LA (A) and remdesivir (B) against various SARS-CoV-2 variants, including Alpha (B.1.1.7), Beta (B.1.351), Delta (B.1.617.2), and Omicron (B.1.1.529) in Vero cells. DMSO (0.1%) was used as solvent control. The mean ± SEM was calculated from duplicate experiments. Confocal images of SARS-CoV-2 N protein (green) and cell nuclei at concentrations near the IC_{50} of LA. The error bars are not visible when they are within the symbols.

triterpenoid saponins in preventing SARS-CoV-2 infection at the stage of membrane fusion. We previously reported that PD, a triterpenoid saponin derived from PG, inhibited SARS-CoV-2 infection and proposed the blockade of membrane fusion as a possible mechanism of action by demonstrating its ability to inhibit a well-known membrane fusion event of spontaneous inhibitory postsynaptic currents in acute brain slices (19). Here, we discovered that LA, a triterpenoid saponin isolated from CL and with a similar chemical composition to PD, exhibited inhibitory activity against SARS-CoV-2. To provide direct evidence that LA blocks the membrane fusion mediated by the S protein of SARS-CoV-2, we established cell fusion assay systems based on S protein-ACE2 interaction. The results from these assays revealed that LA indeed hindered the S-mediated membrane fusion event, thereby preventing SARS-CoV-2 infection.

Cholesterol is an essential component of cell membranes involved in virus-host cell fusion and cell-cell fusion for SARS-CoV-2 entry and pathological syncytium formation (27, 49). Thus, cholesterol-targeting therapeutics have been proposed for the treatment of COVID-19 (50). The role of membrane cholesterol in SARS-CoV-2 infection was highlighted by recent studies showing that 25-hydroxycholesterol inhibits SARS-CoV-2 entry by blocking membrane fusion through depleting accessible cholesterol from the plasma membrane (51–53). It was also reported that exogenously added 27-hydroxycholesterol accumulates in the plasma membrane lipid rafts, leading to the inhibition of SARS-CoV-2 entry (50, 54). Together, these studies suggest that transient changes in cholesterol distribution in plasma membranes can exert inhibitory effects on membrane fusion and viral entry. In this regard, we investigated the effects of LA on membrane cholesterol and observed that upon treatment with LA, cholesterol levels at the plasma and endosomal membranes were significantly increased, implying that LA blocks S-mediated membrane fusion by altering cholesterol distribution in membrane compartments.

In this study, we also explained the structure-activity relationship by comparing the antiviral activity of three different triterpenoid saponins isolated from CL such as LA, LB, and LD. These compounds share structure similarities consisting of a 30-carbon triterpene backbone with a single sugar at position C3 and an oligosaccharide chain attached at position C28, but the number of sugar units and the presence or absence of a branched sugar in the oligosaccharide chain are different (Fig. 1C). Both pSARS-CoV-2 entry assay and cell-to-cell fusion assay identically demonstrated that LA, consisting of linearly linked four sugar residues, exhibited the most potent antiviral activity compared to LB and LD that are composed of a branched and/or a shorter chain of sugar residues, indicating that both length and linearity of the conjugated sugar residues of triterpenoid saponins are critical for such inhibitory actions. Previously, our molecular modeling studies predicted that the triterpene backbone of PD is embedded in the lipid bilayer membrane with an oligosaccharide chain sticking out of the membrane, highlighting the importance of the glycosylated group attached at the C28 position in the antiviral activity (19, 55). Thus, the present study corroborates our previous results, further supporting the idea that the linear sugar residues of triterpenoid saponins create a protrusion from the cell membrane and play critical roles in hindering membrane fusion events. Intriguingly, the potency of LA, LB, and LD against SARS-CoV-2 are well correlated with their ability to increase membrane cholesterol levels (Fig. 2A and 4B and E), raising an interesting possibility that the attached oligosaccharide chain of LA might also be responsible for the alteration of membrane cholesterol. More detailed studies of the relationships of structure and mechanism of action of triterpenoid saponins, including LA are needed to address this hypothesis.

There are many advantages of membrane fusion blockers over other viral entry inhibitors. Because most reported mutations of SARS-CoV-2 variants are clustered near the RBD of S protein, compounds that bind to ancestral S protein and block its interaction with ACE2 might exhibit reduced inhibitory activity against SARS-CoV-2 variants as monoclonal antibodies targeting the RBD of the S protein of ancestral virus showed reduced neutralizing activity against new variants of SARS-CoV-2 (56, 57). Moreover,

SARS-CoV-2 entry inhibitors that specifically act on the interaction between S protein and ACE2 do not provide cross-reactivity to other coronaviruses that recognize different cellular receptors, such as MERS-CoV that uses the receptor dipeptidyl peptidase 4 (DPP4) (58) and novel enveloped viruses that might utilize a different cellular receptor to enter host cells. In contrast, viral membrane fusion blockers have a broader application because the membrane fusion process is shared in all enveloped viruses, including SARS-CoV-2 and its variants. Supporting this notion, we here demonstrated that LA effectively inhibits the infection of the ancestral SARS-CoV-2 and its variants, including Omicron with similar IC_{50} values ranging from 2.23 to 3.37 μM. Another advantage is that, because membrane fusion is a common event in the viral entry pathways, fusion blockers can prevent two main SARS-CoV-2 entry routes with similar efficiency. In agreement with this hypothesis, we found that LA inhibits the cell surface and endosomal pathways of SARS-CoV-2 entry with similar IC_{50} values in experiments using pseudotyped and authentic viruses. It is also important to note that one of the drawbacks of LA is the attached oligosaccharide chain of LA can be hydrolyzed by intestinal bacteria (59). Therefore, it would be better to administer LA via the nasal route in the form of drops or spray rather than oral administration at the early and asymptomatic stages. These ideas need to be evaluated in future studies using animal models.

The S-mediated membrane fusion is critical not only for SARS-CoV-2 entry into host cells but also for syncytium formation. The important roles of syncytium formation in SARS-CoV-2 infection include evasion from neutralizing antibodies and viral spread by cell-to-cell transmission (60, 61). Moreover, syncytia can lead to cell death via apoptosis or pyroptosis, releasing virus particles to reinfect neighboring cells and triggering an inflammatory response (27, 62). Here, we observed that LA effectively inhibited S protein-mediated syncytium formation and cellular apoptosis, indicating that LA could block SARS-CoV-2 pathological effects.

Overall, LA is a natural viral fusion blocker that effectively prevents SARS-CoV-2 and all newly emerging variants from infecting host cells and syncytium formation by hindering the S-mediated membrane fusion. We propose here that LA can be a broad-spectrum antiviral drug not only against SARS-CoV-2 but also against other novel enveloped viral pathogens that might arise in the future.

MATERIALS AND METHODS

Plant material. The aerial parts and roots of *Codonopsis lanceolata* Trautv. (Campanulaceae) used in this study were collected at Daemosan mountain, Seoul, Republic of Korea, in April 2021. The origin of the plant was identified by D.S.J., one of the authors, and voucher specimens (COLA-A-2021 and COLA-R-2021) have been deposited in the Laboratory of Natural Product Medicine, College of Pharmacy, Kyung Hee University, Seoul, Republic of Korea.

Extraction and isolation. The fresh aerial parts (289 g) and roots (209 g) were sliced and extracted in an ultrasonic bath (room temperature for 2 h with 3 L and 2 L of 70% EtOH, respectively) five times. The extracts were filtered and concentrated by a rotary evaporator to give 70% EtOH extracts of the aerial parts (29.4 g, 10.20%) and roots (23.5 g, 11.24%). The eight compounds tested in this study, tangshenoside I (i), ethylsyringin (ii), syringin (iii), sinapaldehyde glucoside (iv), lobetyolin (v), lancemasides A (vi), B (vii), and D (viii), were previously isolated from the roots of CL, and their chemical structures were identified by spectroscopic (^{1}H-nuclear magnetic resonance (NMR), 13C-NMR, 2D-NMR, and/or MS) measurements and by comparing the data with published values (24) (Fig. S3 in Supplemental File 1). The purities of all isolates were determined as >95% by High Performance Liquid Chromatography (HPLC) and/or NMR experiments.

Reagent. Echinocystic acid (purity, ≥95%) was purchased from Sigma-Aldrich.

Cells and viruses. H1299 cells were obtained from the Korean Cell Line Bank (KCLB, South Korea, 25803) and cultured in RPMI 1640 (Gibco, USA). HEK293T and Vero cells were obtained from the American Type Culture Collection (CRL-3216 and CCL-81) and cultured in Dulbecco's Modified Eagle's Medium (DMEM; Corning, USA), respectively. Both culture media were supplemented with 10% fetal bovine serum (FBS) (Gibco, USA) and 1× penicillin-streptomycin solution (HyClone, USA). Cell cultures were incubated at 37°C in a humidified incubator containing 5% CO_2. For viruses, early isolates of SARS-CoV-2 viruses (NCCP43326) and four SARS-CoV-2 variants, including Alpha (NCCP43381), Beta (NCCP43382), Delta (NCCP43390), and Omicron (NCCP43408) were obtained from Korea Disease Control and Prevention Agency (KDCA). These viruses were propagated in Vero E6 cells, and the viral titers were determined by plaque assay using Vero cells. All experiments with these viruses were conducted in an enhanced biosafety level 3 (BSL-3) containment facility at Institut Pasteur Korea as approved by the KDCA.

Production of lentiviral particles and generation of stable cell lines. The full-length SARS-CoV-2 spike sequence from SARS-CoV-2 spike plasmid (a gift from Fang Li, Addgene plasmid number 145032) was cloned into pHR-CMV or pHR-CMV_IRES-EmGFP lentiviral expression plasmid (a gift from A. Radu Aricescu, Addgene plasmid number 113887 and number 113888) via EcoRI and AgeI restriction sites. Lentiviral plasmids encoding ACE2 and TMPRSS2 were cloned and obtained as described in previous work (19). For lentiviral packaging, HEK293T cells were cotransfected with the lentiviral expression plasmids and the packaging plasmid psPAX2 and envelope plasmid pMD2.G using Lipofectamine 3000 (Thermo Fisher, USA) according to the manufacturer's instructions. Supernatants containing the lentivirus were harvested at 24 h and 48 h posttransfection, combined, and filtered through a 0.45 μm-pore-size filter. To generate stable cell lines, H1299 or HEK293T cells plated on 6-well plates with 50% to 60% confluence were incubated for 24 h with 1 mL of the viral supernatants in the presence of Polybrene (Merck, Germany) at a final concentration of 4 μg/mL, followed by replacing with fresh medium and further cultures of additional 2 to 3 days.

Production of SARS-CoV-2 S-pseudotyped lentivirus and pSARS-CoV-2 entry assay. SARS-CoV-2 S-pseudotyped lentiviruses (pSARS-CoV-2) were generated using 2nd generation lentiviral packing system as described in previous work (19). Briefly, HEK293T cells that reached 70 to 80% confluence were transfected with a lentiviral plasmid harboring a gene encoding fly luciferase, psPAX2 packing plasmid, and SARS-CoV-2 S plasmid using Lipofectamine 3000 transfection reagent (Invitrogen, USA) following the manufacturer's instructions. At 24 h and 48 h posttransfection, culture supernatants containing pSARS-CoV-2 virus particles were collected and centrifuged at 500 $\times$ *g* for 5 min to remove the cellular debris and stored at 4°C until use. For the pSARS-CoV-2 entry assay, ACE2$^+$ and ACE2/TMPRSS2$^+$ H1299 cells plated on a 48-well plate with 60% to 80% confluence were pretreated for 1 h with each drug, followed by an overlay of supernatants containing pSARS-CoV-2 virus particles in the presence of each drug. After 24 h of incubation, viral entry efficiency was quantified by measuring the firefly luciferase activity in cell lysates using a luciferase assay system (Promega, USA) and SpectraMax iD5 Multi-Mode Microplate Reader (Molecular Devices, USA).

Dose-response curve analysis by immunofluorescence assay. Vero cells were seeded at 1.2 $\times$ 10^4 cells per well in black, 384-well, μClear plates (Greiner Bio-One, Austria). After 24 h, the cells were transferred into the BSL-3 containment facility and SARS-CoV-2 was added at a multiplicity of infection (MOI) of 0.008 and incubated for an additional 24 h. The cells were then fixed with 4% paraformaldehyde (PFA) and immunostained with an antibody against SARS-CoV-2 nucleocapsid (N) protein, and cell nuclei were visualized with DNA fluorochrome Hoechst 33342. The images were acquired using Operetta high-throughput imaging device (Perkin Elmer) and analyzed using Columbus software (PerkinElmer, Inc. Waltham, MA) to quantify cell numbers and infection ratios. Antiviral activity was normalized to infection control (0.5% DMSO) in each assay plate. DRCs were generated using Prism software (GraphPad). IC_{50} values were measured in duplicates and calculated using nonlinear regression analysis.

Dose-response curve analysis with SARS-CoV-2-Nluc. A549-ACE2-TMPRSS2 cells (1.2 $\times$ 10^4 cells per well) were plated into white 384-well μClear plates (Greiner Bio-One). On the next day, the cells were treated with a 2-fold serial dilution of the compound prepared in DMSO and infected with SARS-CoV-2-Nluc (MOI 0.01) (36). After incubation at 37°C for 24 h, nanoluciferase substrates (Promega) were added to each well, and luciferase signals were measured using a VICTOR3^{TM} multilabel plate reader (PerkinElmer). Cell viability was measured using the CellTiter-Glo Luminescent Cell Viability Assay (Promega, Madison, WI, USA) according to the manufacturer's instructions. The relative luciferase signals of the compound-treated groups were normalized to that of noninfection control (set as 0%) and DMSO-treated groups (set as 100%). The DRCs were generated using Prism6 software (GraphPad, San Diego, CA), and IC_{50} (half-maximal inhibitory concentration) and CC_{50} (half-maximal cytotoxic concentration) values were calculated using a nonlinear regression model.

Cell viability assay. H1299 and Vero cells seeded in a 96-well plate (5 $\times$ 10^3 cells/well) were treated with the indicated concentrations of CL extracts or each compound for 24 h. Subsequently, WST-8 solution (Biomax, South Korea) was added to each well and incubated for 2 h at 37°C in a CO_2 incubator. The absorbance of the water-soluble formazan dye formed was measured at 450 nm using SpectraMax iD5 Multi-Mode Microplate Reader (Molecular Devices, USA). The relative cell viability was expressed as a percentage relative to the untreated control cells.

SARS-CoV-2 Spike-ACE2 binding assay. A recombinant protein containing receptor-binding domain (RBD) of the SARS-CoV2 spike protein fused with GFP (S-RBD-GFP) was produced in Expi293F cells after transfection of pcDNA3-SARS-CoV-2-S-RBD-sfGFP (a gift from Erik Procko, Addgene plasmid number 141184) using the ExpiFectamine^{TM} 293 transfection kit and grown in Expi293 expression medium (Thermo Fisher Scientific, USA) for 4 to 5 days. The culture medium was cleared via centrifugation at 800 $\times$ *g* for 5 min and stored at 4°C until analysis. For the binding assay, ACE2$^+$ H1299 cells were treated with DMSO or indicated concentrations of CL extracts or triterpenoid saponins including LA, LB, and LD for 30 min, followed by incubation with a 1/10 dilution of medium containing S-RBD-GFP for 10 min at 37°C in a CO_2 incubator. ACE2$^+$ H1299 cells were then washed with PBS containing 1% BSA and analyzed for the binding of S-RBD-GFP using an LSRFortessa flow cytometer (BD Biosciences). The data were analyzed using FlowJo software (BD Life Sciences).

S-mediated cell fusion assay using time-lapse microscopy and flow cytometry. For time-lapse microscopy, mRuby2 fluorescence-positive ACE2/TMPRSS2$^+$ H1299 cells were seeded in clear bottom 24-well plates (ibidi, number 82426) overnight, and then treated with DMSO or 10 μM LA for 1 h, followed by adding HEK293T cells expressing EGFP or both S protein and EGFP from a single bicistronic mRNA in (Spike-HEK293T). Time-lapse fluorescence images were acquired at 4 min intervals for 1 h at $\times$40 magnification using a Leica DMi8 microscope (Leica Microsystems, Germany). For flow cytometry assay, mRuby2-

positive ACE2/TMPRSS2$^+$ H1299 cells were seeded in a 12-well plate (2×10^5 cells/well) overnight and treated with DMSO, or 10 μM lancemaside A, B, or D. After incubation for 30 min, 6.5×10^4 cells of EGFP-HEK293T or Spike-HEK293T cells were added and further incubated for 1 h at 37°C in a CO_2 incubator. The cocultures were harvested using trypsin-EDTA and 1×10^4 cells and analyzed by flow cytometry using LSRFortessa (BD Biosciences) to determine the percentage of EGFP and mRuby double-positive cells as a measure of heterologous cell fusion. The data were analyzed using FlowJo software (BD Life Sciences).

Split-GFP assay to detect the S-mediated syncytium formation. ACE2/TMPRSS2$^+$ H1299 cells separately expressing two nonfluorescent fragments of GFP (GFP1-10 and GFP11) (63) were established and equal numbers of these cells were plated in clear bottom 96-well plates (ibidi, number 89626). The next day, the cultures were infected with lentiviral particles expressing SARS-CoV-2 S protein for 6 h and treated with DMSO or various concentrations of LA, followed by incubation for 36 h. The cells were then fixed with 4% paraformaldehyde (PFA) and stained with DAPI (Invitrogen, D1306) to identify the nuclei. Acquisition and automated analysis of fluorescent cell images were carried out using an ImageXpress Pico system (Molecular Devices) with CellReporterXpress software (cell scoring function, 2-channel assay for scoring cells based on the DAPI stained nuclei and GFP images). Nuclei which overlap GFP fluorescence (designated syncytia) and free nuclei were pseudocolored in green and red, respectively, using CellReporterXpress software and the percentage of syncytium formation was calculated as the ratio of green to (green + red) colored nuclei.

Filipin cholesterol staining. Cells grown on glass coverslips were fixed with 4% PFA and then stained with 5 μg/mL filipin-III (Cayman, USA) in PBS containing 1% FBS for 2 h to examine the intracellular distribution of free cholesterol. The stained cells were observed under an LSM 700 confocal microscope (Carl Zeiss, Germany). Signal intensities of plasma membranes were quantified using Image J software (http://imagej.nih.gov/ij/).

Western blotting. Protein samples from the cells of the split-GFP assay (incubation time was prolonged to 72 h) were prepared by dissolving the cultures directly in 2 $\times$ SDS sample buffer and analyzed by Western blot analysis. The primary antibodies used were rabbit anti-cleaved caspase-3 and caspase-9 (Cell Signaling number 9664 and number 52873), and mouse anti-GAPDH (Abcam, ab8245). We used secondary antibodies conjugated with horseradish peroxidase (KPL, USA), and developed the blots using ECL Western Blotting Substrate (Thermo Fisher Scientific, USA). Images of original uncropped Western blots were provided (Fig. S4 in Supplemental File 1).

Comparison of the infectivity of WT and D614G mutant of pSARS-CoV-2. To generate pSARS-CoV-2 harboring D614G mutation on spike protein, a single nucleotide A-to-G substitution was introduced by site-directed mutagenesis into SARS-CoV-2 spike plasmid using the primer sequence 5′-GTGGCCGTGCTGTACCAGGGCGTGAATTGCACCGAGGTG-3′. WT and D614G pSARS-CoV2 viruses were produced as described above. The culture supernatants containing viral particles were filtered on a 0.45 μm pore filter and concentrated by ultracentrifugation at 28,000 rpm for 2 h at 4°C in a Beckman SW28 rotor and an Optima XE-100 Ultracentrifuge (Beckman Coulter). The virus pellets were resuspended in PBS buffer and then viral titers were determined by a qRT-PCR method using a Lentivirus Titration kit (LV900, ABM). The equivalent amount of WT and D614G pSARS-CoV2 viruses were used to infect host cells for the pSARS-CoV-2 entry assay.

Statistical analysis. The data shown in this study are representative of two or three independent experiments and presented as the mean $\pm$ SEM of triplicate samples. The results were analyzed using Student's *t* test and a *P* value less than 0.05 was considered to indicate statistical significance (****, $P < 0.0001$; NS, not significant). Prism v.9.0.0 (GraphPad Software) was used for statistical analyses.

Data availability. Materials are available upon a reasonable request from the corresponding author.

SUPPLEMENTAL MATERIAL

Supplemental material is available online only.

SUPPLEMENTAL FILE 1, PDF file, 0.8 MB.

ACKNOWLEDGMENTS

We appreciate Chanyong Koak for providing the root of *Codonopsis lanceolata*, which motivated the present study. We also thank Haejin Jung and Taek Seung Kim, senior engineer at the Research Solution Center (RSC) in IBS, for performing the flow cytometry analysis and imaging cell-to-cell fusion using a Leica DMi8 microscope, respectively.

Conceptualization, T.Y.K., D.S.J., S.K., and C.J.L.; Experimental execution, T.Y.K., S.J., M.K., Y.E.D., and S.-R.S. Methodology and formal analysis, T.Y.K., S.J.; writing-original draft preparation, T.Y.K., and S.J.; writing-review and editing, T.Y.K., D.S.J., S.K., and C.J.L. All authors read and agreed to the published version of the manuscript.

This work was supported by the Institute for Basic Science (IBS), Center for Cognition and Sociality (IBS-R001-D2) to C.J.L., National Research Foundation of Korea (NRF) with grants funded by the Korean government (MSIT) (NRF-2017M3A9G6068245 and NRF-2022M3A9J1081343 to S.K., and NRF-2019R1A2C1083945 to D.S.J.).

We declare no conflict of interest.

REFERENCES

1. Scovino AM, Dahab EC, Vieira GF, Freire-de-Lima L, Freire-de-Lima CG, Morrot A. 2022. SARS-CoV-2's variants of concern: a brief characterization. Front Immunol 13:834098. https://doi.org/10.3389/fimmu.2022.834098.
2. Aleem A, Akbar Samad AB, Slenker AK. 2022. Emerging variants of SARS-CoV-2 And Novel Therapeutics Against Coronavirus (COVID-19). StatPearls. StatPearls Publishing LLC, Treasure Island (FL).
3. Gowrisankar A, Priyanka TMC, Banerjee S. 2022. Omicron: a mysterious variant of concern. Eur Phys J Plus 137:100. https://doi.org/10.1140/epjp/s13360-021-02321-y.
4. Rahmani S, Rezaei N. 2022. Omicron (B.1.1.529) variant: development, dissemination, and dominance. J Med Virol 94:1787–1788. https://doi.org/10.1002/jmv.27563.
5. Chen KK, Huang DT-N, Huang LM. 2022. SARS-CoV-2 variants - Evolution, spike protein, and vaccines. Biomed J 45:573–579. https://doi.org/10.1016/j.bj.2022.04.006.
6. Du Z, Hong H, Wang S, Ma L, Liu C, Bai Y, Adam DC, Tian L, Wang L, Lau EHY, Cowling BJ. 2022. Reproduction number of the Omicron variant triples that of the Delta variant. Viruses 14:821. https://doi.org/10.3390/v14040821.
7. Biswas S, Mahmud S, Mita MA, Afrose S, Hasan MR, Paul GK, Shimu MSS, Uddin MS, Zaman S, Park MN, Siyadatpanah A, Obaidullah AJ, Saleh MA, Simal-Gandara J, Kim B. 2022. The Emergence of SARS-CoV-2 variants with a lower antibody response: a genomic and clinical perspective. Front Med (Lausanne) 9:825245. https://doi.org/10.3389/fmed.2022.825245.
8. DeGrace MM, Ghedin E, Frieman MB, Krammer F, Grifoni A, Alisoltani A, Alter G, Amara RR, Baric RS, Barouch DH, Bloom JD, Bloyet L-M, Bonenfant G, Boon ACM, Boritz EA, Bratt DL, Bricker TL, Brown L, Buchser WJ, Carreño JM, Cohen-Lavi L, Darling TL, Davis-Gardner ME, Dearlove BL, Di H, Dittmann M, Doria-Rose NA, Douek DC, Drosten C, Edara V-V, Ellebedy A, Fabrizio TP, Ferrari G, Fischer WM, Florence WC, Fouchier RAM, Franks J, García-Sastre A, Godzik A, Gonzalez-Reiche AS, Gordon A, Haagmans BL, Halfmann PJ, Ho DD, Holbrook MR, Huang Y, James SL, Jaroszewski L, Jeevan T, Johnson RM. 2022. Defining the risk of SARS-CoV-2 variants on immune protection. Nature 605:640–652. https://doi.org/10.1038/s41586-022-04690-5.
9. Hoffmann M, Krüger N, Schulz S, Cossmann A, Rocha C, Kempf A, Nehlmeier I, Graichen L, Moldenhauer A-S, Winkler MS, Lier M, Dopfer-Jablonka A, Jäck H-M, Behrens GMN, Pöhlmann S. 2022. The Omicron variant is highly resistant against antibody-mediated neutralization: implications for control of the COVID-19 pandemic. Cell 185:447–456.e11. https://doi.org/10.1016/j.cell.2021.12.032.
10. Hoffmann M, Kleine-Weber H, Schroeder S, Krüger N, Herrler T, Erichsen S, Schiergens TS, Herrler G, Wu N-H, Nitsche A, Müller MA, Drosten C, Pöhlmann S. 2020. SARS-CoV-2 cell entry depends on ACE2 and TMPRSS2 and is blocked by a clinically proven protease inhibitor. Cell 181:271–280.e8. https://doi.org/10.1016/j.cell.2020.02.052.
11. Tang T, Bidon M, Jaimes JA, Whittaker GR, Daniel S. 2020. Coronavirus membrane fusion mechanism offers a potential target for antiviral development. Antiviral Res 178:104792. https://doi.org/10.1016/j.antiviral.2020.104792.
12. Xia S, Liu M, Wang C, Xu W, Lan Q, Feng S, Qi F, Bao L, Du L, Liu S, Qin C, Sun F, Shi Z, Zhu Y, Jiang S, Lu L. 2020. Inhibition of SARS-CoV-2 (previously 2019-nCoV) infection by a highly potent pan-coronavirus fusion inhibitor targeting its spike protein that harbors a high capacity to mediate membrane fusion. Cell Res 30:343–355. https://doi.org/10.1038/s41422-020-0305-x.
13. Huang Y, Yang C, Xu X-F, Xu W, Liu S-W. 2020. Structural and functional properties of SARS-CoV-2 spike protein: potential antivirus drug development for COVID-19. Acta Pharmacol Sin 41:1141–1149. https://doi.org/10.1038/s41401-020-0485-4.
14. Liu S, Xiao G, Chen Y, He Y, Niu J, Escalante CR, Xiong H, Farmar J, Debnath AK, Tien P, Jiang S. 2004. Interaction between heptad repeat 1 and 2 regions in spike protein of SARS-associated coronavirus: implications for virus fusogenic mechanism and identification of fusion inhibitors. Lancet 363:938–947. https://doi.org/10.1016/S0140-6736(04)15788-7.
15. Lu L, Liu Q, Zhu Y, Chan K-H, Qin L, Li Y, Wang Q, Chan JF-W, Du L, Yu F, Ma C, Ye S, Yuen K-Y, Zhang R, Jiang S. 2014. Structure-based discovery of Middle East respiratory syndrome coronavirus fusion inhibitor. Nat Commun 5:3067. https://doi.org/10.1038/ncomms4067.
16. Xia S, Yan L, Xu W, Agrawal AS, Algaissi A, Tseng C-TK, Wang Q, Du L, Tan W, Wilson IA, Jiang S, Yang B, Lu L. 2019. A pan-coronavirus fusion inhibitor targeting the HR1 domain of human coronavirus Spike. Sci Adv 5:eaav4580. https://doi.org/10.1126/sciadv.aav4580.
17. de Vries RD, Schmitz KS, Bovier FT, Predella C, Khao J, Noack D, Haagmans BL, Herfst S, Stearns KN, Drew-Bear J, Biswas S, Rockx B, McGill G, Dorrello NV, Gellman SH, Alabi CA, de Swart RL, Moscona A, Porotto M. 2021. Intranasal fusion inhibitory lipopeptide prevents direct-contact SARS-CoV-2 transmission in ferrets. Science 371:1379–1382. https://doi.org/10.1126/science.abf4896.
18. Newman DJ, Cragg GM. 2020. Natural products as sources of new drugs over the nearly four decades from 01/1981 to 09/2019. J Nat Prod 83:770–803. https://doi.org/10.1021/acs.jnatprod.9b01285.
19. Kim TY, Jeon S, Jang Y, Gotina L, Won J, Ju YH, Kim S, Jang MW, Won W, Park MG, Pae AN, Han S, Kim S, Lee CJ. 2021. Platycodin D, a natural component of Platycodon grandiflorum, prevents both lysosome- and TMPRSS2-driven SARS-CoV-2 infection by hindering membrane fusion. Exp Mol Med 53:956–972. https://doi.org/10.1038/s12276-021-00624-9.
20. Choi JH, Hwang YP, Lee HS, Jeong HG. 2009. Inhibitory effect of Platycodi Radix on ovalbumin-induced airway inflammation in a murine model of asthma. Food Chem Toxicol 47:1272–1279. https://doi.org/10.1016/j.fct.2009.02.022.
21. Lee S, Han EH, Lim M-K, Lee S-H, Yu HJ, Lim YH, Kang S. 2020. Fermented platycodon grandiflorum extracts relieve airway inflammation and cough reflex sensitivity in vivo. J Med Food 23:1060–1069. https://doi.org/10.1089/jmf.2019.4595.
22. Hossen MJ, Kim M-Y, Kim J-H, Cho JY. 2016. *Codonopsis lanceolata*: a review of its therapeutic potentials. Phytother Res 30:347–356. https://doi.org/10.1002/ptr.5553.
23. Seo Y-S, Kim HS, Lee AY, Chun JM, Kim SB, Moon BC, Kwon B-I. 2019. Codonopsis lanceolata attenuates allergic lung inflammation by inhibiting Th2 cell activation and augmenting mitochondrial ROS dismutase (SOD2) expression. Sci Rep 9:2312. https://doi.org/10.1038/s41598-019-38782-6.
24. Du YE, Lee JS, Kim HM, Ahn J-H, Jung IH, Ryu JH, Choi J-H, Jang DS. 2018. Chemical constituents of the roots of Codonopsis lanceolata. Arch Pharm Res 41:1082–1091. https://doi.org/10.1007/s12272-018-1080-9.
25. Crawford KHD, Eguia R, Dingens AS, Loes AN, Malone KD, Wolf CR, Chu HY, Tortorici MA, Veesler D, Murphy M, Pettie D, King NP, Balazs AB, Bloom JD. 2020. Protocol and reagents for pseudotyping lentiviral particles with SARS-CoV-2 Spike protein for neutralization assays. Viruses 12:513. https://doi.org/10.3390/v12050513.
26. Yan VC, Muller FL. 2021. Why remdesivir failed: preclinical assumptions overestimate the clinical efficacy of remdesivir for COVID-19 and Ebola. Antimicrob Agents Chemother 65:e0111721. https://doi.org/10.1128/AAC.01117-21.
27. Sanders DW, Jumper CC, Ackerman PJ, Bracha D, Donlic A, Kim H, Kenney D, Castello-Serrano I, Suzuki S, Tamura T, Tavares AH, Saeed M, Holehouse AS, Ploss A, Levental I, Douam F, Padera RF, Levy BD, Brangwynne CP. 2021. SARS-CoV-2 requires cholesterol for viral entry and pathological syncytia formation. Elife 10:e65962. https://doi.org/10.7554/eLife.65962.
28. Buchrieser J, Dufloo J, Hubert M, Monel B, Planas D, Rajah MM, Planchais C, Porrot F, Guivel-Benhassine F, Van der Werf S, Casartelli N, Mouquet H, Bruel T, Schwartz O. 2020. Syncytia formation by SARS-CoV-2-infected cells. EMBO J 39:e106267.
29. Bussani R, Schneider E, Zentilin L, Collesi C, Ali H, Braga L, Volpe MC, Colliva A, Zanconati F, Berlot G, Silvestri F, Zacchigna S, Giacca M. 2020. Persistence of viral RNA, pneumocyte syncytia and thrombosis are hallmarks of advanced COVID-19 pathology. EBioMedicine 61:103104. https://doi.org/10.1016/j.ebiom.2020.103104.
30. Hooper P, Zaki S, Daniels P, Middleton D. 2001. Comparative pathology of the diseases caused by Hendra and Nipah viruses. Microbes Infect 3:315–322. https://doi.org/10.1016/S1286-4579(01)01385-5.
31. Nardacci R, Perfettini J-L, Grieco L, Thieffry D, Kroemer G, Piacentini M. 2015. Syncytial apoptosis signaling network induced by the HIV-1 envelope glycoprotein complex: an overview. Cell Death Dis 6:e1846. https://doi.org/10.1038/cddis.2015.204.
32. Ozono S, Zhang Y, Ode H, Sano K, Tan TS, Imai K, Miyoshi K, Kishigami S, Ueno T, Iwatani Y, Suzuki T, Tokunaga K. 2021. SARS-CoV-2 D614G spike mutation increases entry efficiency with enhanced ACE2-binding affinity. Nat Commun 12:848. https://doi.org/10.1038/s41467-021-21118-2.
33. Zaman R, Orakzai SA, Yunus A. 1987. Effect of pyrazinamide on serum and urinary uric acid levels. J Pak Med Assoc 37:76–78.
34. Zhang L, Jackson CB, Mou H, Ojha A, Peng H, Quinlan BD, Rangarajan ES, Pan A, Vanderheiden A, Suthar MS, Li W, Izard T, Rader C, Farzan M, Choe H. 2020. SARS-CoV-2 spike-protein D614G mutation increases virion spike density and infectivity. Nat Commun 11:6013. https://doi.org/10.1038/s41467-020-19808-4.
35. Schrors B, Riesgo-Ferreiro P, Sorn P, Gudimella R, Bukur T, Rösler T, Löwer M, Sahin U. 2021. Large-scale analysis of SARS-CoV-2 spike-glycoprotein mutants demonstrates the need for continuous screening of virus isolates. PLoS One 16:e0249254. https://doi.org/10.1371/journal.pone.0249254.

36. Rihn SJ, Merits A, Bakshi S, Turnbull ML, Wickenhagen A, Alexander AJT, Baillie C, Brennan B, Brown F, Brunker K, Bryden SR, Burness KA, Carmichael S, Cole SJ, Cowton VM, Davies P, Davis C, De Lorenzo G, Donald CL, Dorward M, Dunlop JI, Elliott M, Fares M, da Silva Filipe A, Freitas JR, Furnon W, Gestuveo RJ, Geyer A, Giesel D, Goldfarb DM, Goodman N, Gunson R, Hastie CJ, Herder V, Hughes J, Johnson C, Johnson N, Kohl A, Kerr K, Leech H, Lello LS, Li K, Lieber G, Liu X, Lingala R, Loney C, Mair D, McElwee MJ, McFarlane S, Nichols J. 2021. A plasmid DNA-launched SARS-CoV-2 reverse genetics system and coronavirus toolkit for COVID-19 research. PLoS Biol 19:e3001091. https://doi.org/10.1371/journal.pbio.3001091.
37. Pitts J, Li J, Perry JK, Du Pont V, Riola N, Rodriguez L, Lu X, Kurhade C, Xie X, Camus G, Manhas S, Martin R, Shi P-Y, Cihlar T, Porter DP, Mo H, Maiorova E, Bilello JP. 2022. Remdesivir and GS-441524 retain antiviral activity against Delta, Omicron, and other emergent SARS-CoV-2 variants. Antimicrob Agents Chemother 66:e0022222. https://doi.org/10.1128/aac.00222-22.
38. Vangeel L, Chiu W, De Jonghe S, Maes P, Slechten B, Raymenants J, André E, Leyssen P, Neyts J, Jochmans D. 2022. Remdesivir, Molnupiravir and Nirmatrelvir remain active against SARS-CoV-2 Omicron and other variants of concern. Antiviral Res 198:105252. https://doi.org/10.1016/j.antiviral.2022.105252.
39. Adeleye OA, Bamiro OA, Bakre LG, Odeleye FO, Adebowale MN, Okunye OL, Sodeinde MA, Adebona AC, Menaa F. 2022. Medicinal Plants with Potential Inhibitory Bioactive Compounds against Coronaviruses. Adv Pharm Bull 12:7–16. https://doi.org/10.34172/apb.2022.003.
40. Benarba B, Pandiella A. 2020. Medicinal Plants as Sources of Active Molecules Against COVID-19. Front Pharmacol 11:1189. https://doi.org/10.3389/fphar.2020.01189.
41. Lee M, Park J, Cho IH. 2022. Target-Specific drug discovery of natural products against SARS-CoV-2 life cycle and cytokine storm in COVID-19. Am J Chin Med 50:927–959. https://doi.org/10.1142/S0192415X22500380.
42. Ebob OT, Babiaka SB, Ntie-Kang F. 2021. Natural Products as Potential Lead Compounds for Drug Discovery Against SARS-CoV-2. Nat Prod Bioprospect 11:611–628. https://doi.org/10.1007/s13659-021-00317-w.
43. Diniz LRL, Perez-Castillo Y, Elshabrawy HA, Filho CdSMB, de Sousa DP. 2021. Bioactive terpenes and their derivatives as potential SARS-CoV-2 proteases inhibitors from molecular modeling studies. Biomolecules 11:74. https://doi.org/10.3390/biom11010074.
44. Falade VA, Adelusi TI, Adedotun IO, Abdul-Hammed M, Lawal TA, Agboluaje SA. 2021. In silico investigation of saponins and tannins as potential inhibitors of SARS-CoV-2 main protease (M(pro)). In Silico Pharmacol 9:9. https://doi.org/10.1007/s40203-020-00071-w.
45. Sinha SK, Shakya A, Prasad SK, Singh S, Gurav NS, Prasad RS, Gurav SS. 2021. An in-silico evaluation of different Saikosaponins for their potency against SARS-CoV-2 using NSP15 and fusion spike glycoprotein as targets. J Biomol Struct Dyn 39:3244–3255. https://doi.org/10.1080/07391102.2020.1762741.
46. Yang R, Liu H, Bai C, Wang Y, Zhang X, Guo R, Wu S, Wang J, Leung E, Chang H, Li P, Liu T, Wang Y. 2020. Chemical composition and pharmacological mechanism of Qingfei Paidu Decoction and Ma Xing Shi Gan Decoction against Coronavirus Disease 2019 (COVID-19): in silico and experimental study. Pharmacol Res 157:104820. https://doi.org/10.1016/j.phrs.2020.104820.
47. Yi Y, Li J, Lai X, Zhang M, Kuang Y, Bao Y-O, Yu R, Hong W, Muturi E, Xue H, Wei H, Li T, Zhuang H, Qiao X, Xiang K, Yang H, Ye M. 2022. Natural triterpenoids from licorice potently inhibit SARS-CoV-2 infection. J Adv Res 36:201–210. https://doi.org/10.1016/j.jare.2021.11.012.
48. Li H, Cheng C, Shi S, Wu Y, Gao Y, Liu Z, Liu M, Li Z, Huo L, Pan X, Liu S, Song G. 2022. Identification, optimization, and biological evaluation of 3-O-β-chacotriosyl ursolic acid derivatives as novel SARS-CoV-2 entry inhibitors by targeting the prefusion state of spike protein. Eur J Med Chem 238:114426. https://doi.org/10.1016/j.ejmech.2022.114426.
49. Barrantes FJ. 2022. The constellation of cholesterol-dependent processes associated with SARS-CoV-2 infection. Prog Lipid Res 87:101166. https://doi.org/10.1016/j.plipres.2022.101166.
50. Palacios-Rápalo SN, De Jesús-González LA, Cordero-Rivera CD, Farfan-Morales CN, Osuna-Ramos JF, Martínez-Mier G, Quistián-Galván J, Muñoz-Pérez A, Bernal-Dolores V, Del Ángel RM, Reyes-Ruiz JM. 2021. Cholesterol-rich lipid rafts as platforms for SARS-CoV-2 entry. Front Immunol 12:796855. https://doi.org/10.3389/fimmu.2021.796855.
51. Wang S, Li W, Hui H, Tiwari SK, Zhang Q, Croker BA, Rawlings S, Smith D, Carlin AF, Rana TM. 2020. Cholesterol 25-Hydroxylase inhibits SARS-CoV-2 and other coronaviruses by depleting membrane cholesterol. EMBO J 39:e106057. https://doi.org/10.15252/embj.2020106057.
52. Zang R, Case JB, Yutuc E, Ma X, Shen S, Gomez Castro MF, Liu Z, Zeng Q, Zhao H, Son J, Rothlauf PW, Kreutzberger AJB, Hou G, Zhang H, Bose S, Wang X, Vahey MD, Mani K, Griffiths WJ, Kirchhausen T, Fremont DH, Guo H, Diwan A, Wang Y, Diamond MS, Whelan SPJ, Ding S. 2020. Cholesterol 25-hydroxylase suppresses SARS-CoV-2 replication by blocking membrane fusion. Proc Natl Acad Sci U S A 117:32105–32113. https://doi.org/10.1073/pnas.2012197117.
53. Zu S, Deng Y-Q, Zhou C, Li J, Li L, Chen Q, Li X-F, Zhao H, Gold S, He J, Li X, Zhang C, Yang H, Cheng G, Qin C-F. 2020. 25-Hydroxycholesterol is a potent SARS-CoV-2 inhibitor. Cell Res 30:1043–1045. https://doi.org/10.1038/s41422-020-00398-1.
54. Marcello A, Civra A, Milan Bonotto R, Nascimento Alves L, Rajasekharan S, Giacobone C, Caccia C, Cavalli R, Adami M, Brambilla P, Lembo D, Poli G, Leoni V. 2020. The cholesterol metabolite 27-hydroxycholesterol inhibits SARS-CoV-2 and is markedly decreased in COVID-19 patients. Redox Biol 36:101682. https://doi.org/10.1016/j.redox.2020.101682.
55. Jang Y, Young Kim T, Jeon S, Lim H, Lee J, Kim S, Justin Lee C, Han S. 2022. Synthesis and structure-activity relationship study of saponin-based membrane fusion inhibitors against SARS-CoV-2. Bioorg Chem 127:105985. https://doi.org/10.1016/j.bioorg.2022.105985.
56. Bekliz M, Adea K, Vetter P, Eberhardt CS, Hosszu-Fellous K, Vu D-L, Puhach O, Essaidi-Laziosi M, Waldvogel-Abramowski S, Stephan C, L'Huillier AG, Siegrist C-A, Didierlaurent AM, Kaiser L, Meyer B, Eckerle I. 2022. Neutralization capacity of antibodies elicited through homologous or heterologous infection or vaccination against SARS-CoV-2 VOCs. Nat Commun 13:3840. https://doi.org/10.1038/s41467-022-31556-1.
57. Takashita E, Kinoshita N, Yamayoshi S, Sakai-Tagawa Y, Fujisaki S, Ito M, Iwatsuki-Horimoto K, Chiba S, Halfmann P, Nagai H, Saito M, Adachi E, Sullivan D, Pekosz A, Watanabe S, Maeda K, Imai M, Yotsuyanagi H, Mitsuya H, Ohmagari N, Takeda M, Hasegawa H, Kawaoka Y. 2022. Efficacy of antibodies and antiviral drugs against COVID-19 Omicron Variant. N Engl J Med 386:995–998. https://doi.org/10.1056/NEJMc2119407.
58. Mou H, Raj VS, van Kuppeveld FJM, Rottier PJM, Haagmans BL, Bosch BJ. 2013. The receptor binding domain of the new Middle East respiratory syndrome coronavirus maps to a 231-residue region in the spike protein that efficiently elicits neutralizing antibodies. J Virol 87:9379–9383. https://doi.org/10.1128/JVI.01277-13.
59. Shan J, Zou J, Xie T, Kang A, Zhou W, Deng H, Mao Y, Di L, Wang S. 2015. Pharmacokinetics, intestinal absorption and microbial metabolism of single platycodin D in comparison to Platycodi radix extract. Pharmacogn Mag 11:750–755. https://doi.org/10.4103/0973-1296.165576.
60. Rajah MM, Bernier A, Buchrieser J, Schwartz O. 2022. The mechanism and consequences of SARS-CoV-2 spike-mediated fusion and syncytia formation. J Mol Biol 434:167280. https://doi.org/10.1016/j.jmb.2021.167280.
61. Zeng C, Evans JP, King T, Zheng YM, Oltz EM, Whelan SP, Saif LJ, Peeples ME, Liu SL. 2022. SARS-CoV-2 spreads through cell-to-cell transmission. Proc Natl Acad Sci U S A 119:e2111400119. https://doi.org/10.1073/pnas.2111400119.
62. Santana MF, Pinto RAdA, Marcon BH, Medeiros LCASd, Morais TBdNd, Dias LC, Souza LPd, Melo GCd, Monteiro WM, Lacerda MVG, Val FA, Lalwani PJ, Ferreira LCdL. 2021. Pathological findings and morphologic correlation of the lungs of autopsied patients with SARS-CoV-2 infection in the Brazilian Amazon using transmission electron microscopy. Rev Soc Bras Med Trop 54:e0850.
63. Buchrieser J, Dufloo J, Hubert M, Monel B, Planas D, Rajah MM, Planchais C, Porrot F, Guivel-Benhassine F, Van der Werf S, Casartelli N, Mouquet H, Bruel T, Schwartz O. 2021. Syncytia formation by SARS-CoV-2-infected cells. EMBO J 40:e107405. https://doi.org/10.15252/embj.2020107405.